# Towards parameterizing eddy-mediated transport of Warm Deep Water across the Weddell Sea continental slope

Nicolas Dettling[a] , Martin Losch[a] , Friederike Pollmann[b] , Torsten Kanzow[a]

[a] *Alfred Wegener Institute Helmholtz Centre for Polar and Marine Research,* [b] *Universität Hamburg*

*Corresponding author*: Nicolas Dettling, nicolas.dettling@awi.de

ABSTRACT: The transport of Warm Deep Water (WDW) onto the Weddell Sea continental shelf is associated with a heat flux and strongly contributes to the melting of Antarctic ice shelves. The small radius of deformation at high latitudes makes it difficult to accurately represent the eddy-driven component of onshore WDW transport in coarse-resolution ocean models so that a parameterization becomes necessary. The Gent and McWilliams/Redi (GM/Redi) scheme was designed to parameterize mesoscale eddies in the open ocean. Here, it is assessed to what extent the GM/Redi scheme can generate a realistic transport of WDW across the Weddell Sea continental slope. To this end, the eddy parameterization is applied to a coarse-resolution idealized model of the Weddell Sea continental shelf and slope, and its performance is evaluated against a high-resolution reference simulation. With the GM/Redi parameterization applied, the coarse model simulates a shoreward WDW transport with a heat transport that matches the high-resolution reference and both the hydrographic mean fields and the mean slopes of the isopycnals are improved. A successful application of the GM/Redi parameterization is only possible by reducing the GM diffusivity over the continental slope by an order of magnitude compared to the open ocean value to account for the eddy-suppressing effect of the topographic slope. When the influence of topography on the GM diffusivity is neglected, the coarse model with the parameterization either under or overestimates the shoreward heat flux. These results motivate the incorporation of slope-aware eddy parameterizations into regional and global ocean models.

SIGNIFICANCE STATEMENT: Mesoscale eddies drive warm water across the continental slope and onto the continental shelf of the Weddell Sea, where it melts the adjacent Antarctic ice shelves. This process is not resolved in ocean models employing a coarse horizontal resolution akin to state-of-the-art climate models. This work addresses this issue by modifying and applying a well-established eddy parameterization to this specific case. The parameterization works particularly well when it accounts for the effect of sloping topography, over which eddy transports are weaker. We expect this modification also to be of benefit to regional and global models.

## 1. Introduction

Antarctic ice shelf and land ice masses are declining in response to climate change (e.g. Cook et al. 2005; Rignot et al. 2014; Joughin et al. 2014; Rignot et al. 2019; Joughin et al. 2021) with implications for global climate (Bronselaer et al. 2018) and sea level rise (DeConto and Pollard 2016; Pan et al. 2021). A major contributor is the transport of warm Circumpolar Deep Water (CDW) onto the Antarctic continental shelf producing basal melting of adjacent ice shelves (Jacobs et al. 1992; Rignot and Jacobs 2002; Pritchard et al. 2012). This results in a thinning and retreat of ice shelves exposed to the warm water, which reduces their buttressing effect and accelerates the mass release of marine-terminating glaciers into the ocean (DeConto and Pollard 2016; Paolo et al. 2015).

In the Weddell Sea, the onshore transport of Warm Deep Water (WDW), a derivative of CDW formed through mixing with colder and fresher water within the Weddell Gyre (Vernet et al. 2019), is concentrated at locations where dense water spills over the continental shelf and is topographically steered down the continental slope (Morrison et al. 2020). Indeed, observations within the Filchner Trough, a major pathway for the export of dense water from the Weddell Sea Continental Shelf, show a coherence between down-slope transport of dense waters and onshore WDW transport (Darelius et al. 2023).

On the Weddell Sea continental shelf, winter surface cooling and salt rejection during sea ice formation transforms cold and fresh Antarctic Surface Water (AASW) into denser High-Salinity Shelf Water (HSSW), some of which then circulates through the Filchner and Ronne ice shelf cavities (Gordon et al. 2001; Nicholls et al. 2001, 2009; Hattermann et al. 2012; Janout et al. 2021). HSSW induces basal melting at the ice shelf-ocean interface where it is transformed into the even denser Ice Shelf Water (ISW) (Jenkins and Doake 1991; Jacobs et al. 1992; Orsi et al. 1999; Foldvik et al. 2004). The dense water subsequently propagates down the continental slope into the abyssal ocean while entraining WDW (Orsi et al. 1999; Gordon et al. 2001; Nicholls et al. 2009). The resulting Weddell Sea Bottom Water (WSBW) forms the densest and most oxygenated contribution to the Antarctic Bottom Water (AABW), which flows northward as the lower limb of the Meridional Overturning Circulation (MOC) (Fahrbach et al. 1995; Gordon et al. 2001; Orsi and Whitworth III 2005).

Together with Ekman convergence and downwelling in response to alongshore winds, the dense water export sets up a characteristic V-shaped isopycnal structure of the Antarctic Slope Front (ASF) (Jacobs 1991; Gill 1973). The ASF separates the continental shelf from Warm Deep Water (WDW) and its offshore flank is associated with the Antarctic Slope Current (ASC) flowing westward along the continental shelf break (Thompson et al. 2018).

The down-slope flow of dense water creates an isopycnal connection between the continental slope and shelf so that no work against buoyancy forces is required to move a water parcel onto the shelf. The continental slope, over which the thickness of isopycnal layers decreases towards the continental shelf, forms a dynamic barrier by imposing a gradient in potential vorticity (PV) (Thompson et al. 2014). Baroclinic instability at the AABW-WDW interface drives a convergence of along-slope momentum and eddy kinetic energy (EKE) in the WDW layer, which allows overcoming this PV gradient (Stewart and Thompson 2016). Other drivers of shoreward WDW transport include residual tidal flow (Wang et al. 2013), interactions of the ASC with submarine troughs and Rossby wave propagation therein (St-Laurent et al. 2013), bottom boundary layer transport (Wåhlin et al. 2012), and wind forcing (Hellmer et al. 2012; Darelius et al. 2016; Daae et al. 2017; Ryan et al. 2017).

Capturing eddy-driven exchanges across the ASF is challenging for numerical ocean models because the small deformation radius at high latitudes can only be resolved at fine horizontal resolutions. For an ocean model to resolve the first baroclinic radius of deformation on a continental shelf and slope at a latitude of 65°S requires a grid resolution of approximately 1 km (Hallberg 2013), much higher than currently feasible in global climate models. Idealized numerical experiments representing the Antarctic continental slope and shelf confirm that a horizontal resolution on the order of $\mathcal{O}(1\text{ km})$ is necessary to resolve eddies and capture the associated dynamical processes (St-Laurent et al. 2013; Stewart and Thompson 2015).

When eddies are not resolved, a parameterization of their effects on the model solution is required. For this purpose, a combination of the Gent and McWilliams (GM, Gent and McWilliams 1990) and the Redi (Redi 1982) scheme is commonly used. The GM scheme reduces isopycnal slopes by means of an advective tracer flux where the advective velocity, often labeled bolus velocity, is a function of the slope of the local isentropic surface. The Redi scheme in turn imposes downgradient diffusion of tracers along neutral surfaces, representing isopycnal diffusion of mesoscale eddies (Redi 1982). Both schemes require setting a transfer coefficient, the thickness or GM diffusivity $\kappa_{GM}$, and the isopycnal or Redi diffusivity $\kappa_{Redi}$.

Initially often set constant, it is clear that the GM and Redi diffusivities should vary in space and time. Several schemes to compute a spatially varying GM coefficient have been proposed based on Mixing Length Theory, in which the diffusivity is related to the product of an eddy length scale and velocity (e.g. Green 1970; Stone 1972; Visbeck et al. 1997; Cessi 2008; Eden and Greatbatch 2008; Jansen et al. 2015). Other schemes derive from the dynamical restratification of mixed-layer instabilities (Fox-Kemper and Ferrari 2008) or from properties of the eddy stress tensor (Marshall et al. 2012). In a subclass of schemes, the GM diffusivity is related to the sub-grid eddy energy (e.g. Cessi 2008; Eden and Greatbatch 2008; Marshall et al. 2012; Jansen et al. 2015).

Frameworks for spatially varying estimates of $\kappa_{GM}$ are usually developed for the case of a flat bottom. Sloping bathymetry, however, influences baroclinic instability depending on the ratio between topographic and isopycnal slope $\delta = s_{topo}/s_{iso}$ (Blumsack and Gierasch 1972; Mechoso 1980; Isachsen 2011; Brink and Cherian 2013). For $\delta < 0$, the bottom slope has a stabilizing effect so that growth rates and length scales reduce with $|\delta|$. When isopycnals moderately slope in the same direction as the bathymetry ($0 < \delta < 1$), the bottom slope acts to destabilize the flow with maximum growth rates obtained for $\delta = 0.5$. Finally, in the case of topographic slopes steeper than the slope of the isopycnals ($\delta > 1$), the growth of instability is entirely suppressed.

Within the ASF, isopycnal slopes tilt both in the same and opposite direction compared to the continental slope (Le Paih et al. 2020). In a process model of the ASF and ASC, Stewart and Thompson (2013) infer reduced diffusivities over the continental slope where $\delta < 0$. Scalings that diagnose the eddy diffusivity from the output of process model simulations of continental slopes perform better when they incorporate information about the topographic slope for both $\delta < 0$ and $\delta > 0$ (Wei and Wang 2021; Wei et al. 2022). Nevertheless, modifications to make the GM/Redi scheme slope-aware remain to be implemented and tested in numerical ocean models and have not been applied in the context of down-slope flows of dense water.

In this work, we apply the GM/Redi parameterization to a numerical ocean model representing the ASF and address the following questions:

1. Does the GM/Redi parameterization for mesoscale eddies reproduce eddy-driven shoreward heat flux associated with the presence of WDW?
2. What is the effect of the GM/Redi parameterization on the simulated hydrographic fields?
3. What are suitable choices for the diffusivities within the GM/Redi scheme to represent the exchange of heat across the continental slope?

For this purpose, we use an idealized model of the Weddell Sea continental slope and shelf and compare high and low-resolution simulations with and without the GM/Redi parameterization. The model setup and parameterization are described in section 2, the performance of the GM/Redi scheme using different diffusivity estimates is evaluated in section 3, followed by a discussion and conclusion in section 4.

## 2. Model setup and analysis

For this work, an idealized model of the Weddell Sea continental slope and shelf is set up. The configuration closely resembles the one described in Stewart and Thompson (2016), for which we will only give a brief description and refer the reader to the original publication for more details. As a reference, we run the model at high-resolution resolving the first baroclinic radius of deformation, and then compare the outcome to a coarse-resolution simulation in which the Rossby radius is not resolved. Subsequently, we add the GM/Redi parameterization at coarse resolution and investigate its influence on cross-slope heat fluxes and the hydrographic mean state.

### *a. Reference Simulations*

All experiments are performed using the hydrostatic version of the Massachusetts Institute of Technology general circulation model (MITgcm, Marshall et al. 1997; MITgcm Group 2023). The domain has a horizontal extent of 450 x 400 km, featuring periodic boundaries in the $y$-direction and closed boundaries in the $x$-direction. The bathymetry of the Weddell Sea continental slope is represented through an idealized, meridionally homogeneous slope connecting a 500 m deep shelf section to the ocean bottom at 3000 m depth (Fig.1). At the surface, the model is forced by a time-invariant meridional wind stress profile $\tau_y$ with a maximum stress of $\tau_{max} = -0.075$ N m$^{-2}$ representing northward wind. Over the first 50 km of the shelf, salt is injected at the surface at a rate of $s_{surf} = 2.5$ mg m$^{-2}$ s$^{-1}$ to produce dense water. In order to maintain realistic Antarctic Surface Water conditions, a two-equation thermodynamic sea ice model (Schmidt et al. 2004) is used. Here, surface heat and salt fluxes representing freezing and melting are determined from surface temperature and salinity. Within a 50 km-wide sponge layer at the open ocean boundary, velocities are restored to zero and temperature and salinity are restored to the initial profiles with time scales of 27 and 54 days respectively. For the experiments, we select a nonlinear equation of state of McDougall et al. (2003) and a 3rd-order direct space-time advection scheme with flux-limiting. The non-local K-Profile parameterization (KPP) (Large et al. 1994) represents vertical mixing in the surface boundary layer and the ocean interior. At the bottom, momentum is extracted by bottom drag parameterized using a linear bottom drag coefficient of $r_b = 10^{-3}$ m s$^{-1}$. Here, the absence of along-slope topographic variations and the associated topographic form drag requires setting an untypically large bottom drag coefficient to simulate ASC velocities in the range of observed

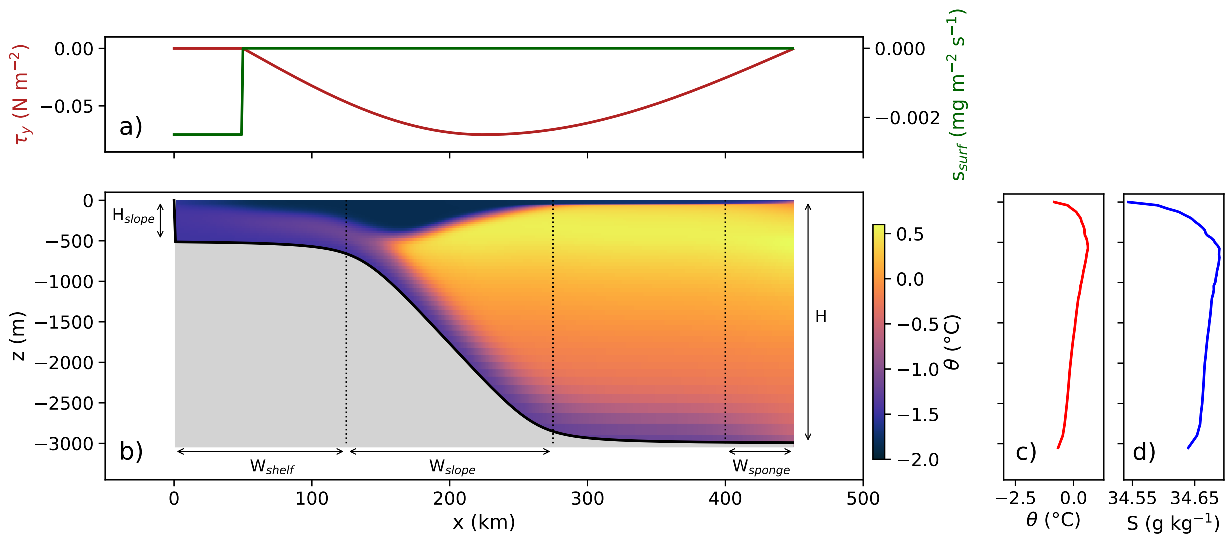


FIG. 1. Input profiles for surface salt flux $s_{surf}$ and meridional wind stress $\tau_y$ (a), topographic slope and along-slope and time-averaged potential temperature $\theta$ at 1 km resolution (b), initial and restoring profiles of potential temperature (c) and salinity $S$ (d).

values. The model is run on an $f$-plane with $\beta = 0$ since the vorticity gradient resulting from the sloping topography is 100 times larger than the change in planetary vorticity. All simulations are initialized from rest using profiles of potential temperature $\theta$ and salinity $S$ representative of the western Weddell Sea (Thompson and Heywood 2008). The model is then integrated with a horizontal grid spacing of 10 km for 40 years after which mean kinetic and potential energies have stabilized and no drift in the domain-averaged temperature and salinity is observed. This coarse resolution ensures that eddies are mostly unresolved over the continental slope while the slope is still represented by a reasonable number of 15 grid points. To obtain the high-resolution reference simulation, the output fields are interpolated to a horizontal resolution of 2 km after which the model is run to equilibrium again. This procedure is then repeated for a horizontal resolution of 1 km. Further refinements in resolution did not produce major changes to the model solution, and therefore, the simulation with a resolution of 1 km will serve as our reference. The numerical parameters of the reference simulation are summarized in table 1.

TABLE 1. Parameter choices for the high-resolution reference simulation.

| | Value | Description |
|---|---|---|
| $nx, ny, nz$ | 450, 400, 77 | Number of grid points in x,y,z direction |
| $dx, dy$ | 1 km, 1 km | Horizontal grid spacing |
| $dz$ | 13-100 m | Vertical grid spacing |
| $dt$ | 180 s | Time step |
| $L_x$ | 450 km | Zonal domain size |
| $L_y$ | 400 km | Meridional domain size |
| $H$ | 3000 m | Max. ocean depth |
| $H_s$ | 500 m | Shelf depth |
| $W_{shelf}$ | 125 km | Shelf width |
| $X_s$ | 200 km | Slope center |
| $\gamma_s$ | 0.05 | Slope scaling factor |
| $W_{slope}$ | 150 km | Slope width |
| $W_{sponge}$ | 50 km | Sponge layer width |
| $T_{hydro}$ | 54 d | Hydrographic restoring time scale |
| $T_{velocity}$ | 27 d | Velocity restoring time scale |
| $s_{surf}$ | 2.5 mg m$^{-2}$ s$^{-1}$ | Shelf salt input |
| $W_{salt}$ | 50 km | Width of salt input region |
| $\tau_{max}$ | -0.075 N m$^{-2}$ | Max. meridional wind stress |
| $X_w$ | 225 km | Position of max. wind stress |
| $r_b$ | $1{\cdot}10^{-3}$ m s$^{-1}$ | Linear drag coefficient |
| $A_z$ | $3{\cdot}10^{-4}$ m$^2$ s$^{-1}$ | Vertical viscosity |
| $A_h$ | 12 | Horizontal viscosity |
| $A_{4grid}$ | 0.1 | Grid-scaled biharmonic viscosity |
| $C_{4leith}$ | 1.0 | Leith biharmonic viscosity factor (vorticity part) |
| $\mathrm{C}_{4leithD}$ | 1.0 | Leith biharmonic viscosity factor (divergence part) |
| $\kappa_z$ | $5 \cdot 10^{-6}$ m$^2$ s$^{-1}$ | Vertical diffusivity |
| $g$ | 9.81 m$^2$ s$^{-1}$ | Gravitational constant |
| $\rho_0$ | 1000 kg m$^{-3}$ | Reference density |
| $f_0$ | $-1.31{\cdot}10^{-4}$ s$^{-1}$ | Coriolis parameter |

### *b. Gent-McWilliams/Redi parameterization*

To investigate the parameterization of mesoscale eddies, we extend the 10 km resolution runs by another 40 years while employing the GM/Redi parameterization. In the GM scheme, a non-divergent stream function, the bolus stream function $\psi_{bolus}$, is computed from the isopycnal slopes $s_{iso,x} = (\frac{\partial\sigma}{\partial x})/(-\frac{\partial\sigma}{\partial z})$ so that

$$\psi_{bolus} = -\kappa_{GM} \cdot s_{iso,x}. \tag{1}$$

Note that the GM scheme acts both in the $x$- and $y$-direction. Because of the symmetry of forcing and topography in the $y$-direction, we describe only the $x$-direction here. The zonal and meridional components $u^*$, $v^*$ of the bolus velocity $\mathbf{u}^*$ are then computed by taking the vertical derivative of the bolus stream function. Finally, the advective flux divergence $F_{GM}$ for an arbitrary tracer $\phi$ is added to the right-hand side (RHS) of the prognostic tracer equations in the form:

$$F_{GM} = -\nabla \cdot (\phi \mathbf{u}^*). \tag{2}$$

The Redi scheme introduces a diffusion term into the RHS of the tracer equations of the form:

$$\nabla \cdot (\kappa_{Redi} \mathbf{K}_{Redi} \nabla \phi) \,. \tag{3}$$

Here, $\mathbf{K}_{Redi}$ is a tensor rotating $\nabla\phi$ along isopycnal surfaces. To avoid numerical instability in the presence of large isopycnal slopes, we use the tapering scheme of Gerdes et al. (1991). No major differences were observed when testing other tapering schemes.

### *c. Simulation analysis*

For analysis, monthly averages of the last 5 simulation years are used. Eulerian mean and eddy across-slope heat and salt transports are diagnosed as

$$F_{\theta,mean} = -c_p \rho_0 \int_y \int_z \overline{u} \cdot \overline{\theta} \; dz \; dy, \tag{4}$$

$$F_{\theta,eddy} = -c_p \rho_0 \int_y \int_z \overline{u'\theta'} dz \; dy, \tag{5}$$

$$F_{S,mean} = -\rho_0 \int_y \int_z \overline{u} \cdot \overline{S} dz \; dy, \tag{6}$$

$$F_{S,eddy} = -\rho_0 \int_y \int_z \overline{u'S'} dz \; dy, \tag{7}$$

where the overbar denotes an average in time and along-slope direction, $c_p$ is the specific heat capacity of water, and $\rho_0$ is the reference density. Here, the covariance term between eddy velocity

$u'$ and an arbitrary quantity $\gamma$ is computed in the form

$$\overline{u'\gamma'} = \overline{u\gamma} - \overline{u} \cdot \overline{\gamma}. \tag{8}$$

The across-slope heat fluxes associated with the GM/Redi parameterization are

$$F_{\theta,GM} = -c_p \rho_0 \int_y \int_z (u^* \cdot \theta) \; dz \; dy, \tag{9}$$

$$F_{\theta,Redi} = -c_p \rho_0 \int_y \int_z (\kappa_{Redi} \cdot \frac{\partial \theta}{\partial x} + \kappa_{Redi} \cdot \frac{\partial \theta}{\partial z} \cdot s_{iso,x}) \; dz \; dy, \tag{10}$$

$$F_{\theta,GM/Redi} = F_{\theta,GM} + F_{\theta,Redi}. \tag{11}$$

Additionally, we compute the eddy kinetic energy (EKE) as

$$EKE = \frac{1}{2} \left( \overline{u'^2} + \overline{v'^2} \right). \tag{12}$$

Barotropic and baroclinic ASC velocities $v_{bt}$ and $v_{bc}$, respectively, are diagnosed as

$$v_{bt} = \overline{v}^z, \tag{13}$$

$$v_{bc} = v - \overline{v}^z, \tag{14}$$

where $\overline{v}^z$ is the vertically averaged along-slope velocity. Further, the difference between the coarse resolution simulation field $\overline{\phi}_{coarse}$ and the coarse-grained high-resolution field $\overline{\phi}_{fine,cg}$ are quantified by calculating the Root Mean Square Difference (RMSD)

$$RMSD = \sqrt{\sum_{x,z} \left( \overline{\phi}_{coarse} - \overline{\phi}_{fine,cg} \right)^2}. \tag{15}$$

Finally, we diagnose the residual overturning by computing a stream function $\psi$ from the transport in 160 layers of potential density $\sigma$ (as in e.g. Döös and Webb 1994; Hallberg and Gnanadesikan 2006; Abernathey et al. 2011):

$$\psi_{res} = \overline{\int_\sigma (uh) \; d\sigma}, \tag{16}$$

where $h = -\partial z/\partial\sigma$ is the thickness of the selected potential density layers. We then map the stream function back to $z$-coordinates using the mean thickness of the potential density layers. This approach has been shown to be formally equivalent to computing the transferred Eulerian-mean (TEM) overturning circulation (McIntosh and McDougall 1996). $\psi$ contains the transport contributions of the Eulerian-mean and eddy overturning circulation. To isolate the eddy component of the overturning, we decompose $\psi$ so that:

$$\psi_{eddy} = \psi_{res} - \psi_{mean}, \tag{17}$$

where $\psi_{mean}$ is the Eulerian-mean transport stream function

$$\psi_{mean} = \int_z (\overline{u})\, dz. \tag{18}$$

## 3. Results

*a. Model solutions at high and coarse resolution*

We start by discussing the differences in the model solutions at horizontal resolutions of 1 and 10 km, which a suitable parameterization has to overcome. We note here, that running the model at a resolution of 1 km increases the computational cost by a factor of 600 compared to the resolution of 1 km.

In the reference simulation, Antarctic Surface Water (AASW) is maintained by interactions with the simplified thermodynamic sea ice model (Fig. 2a-b). The northward wind stress leads to shoreward Ekman transport resulting in a depression of the isopycnals where the surface water converges over the shelf break. The salt input over the shelf produces dense water flowing down the continental slope in the form of a gravity current. The warm and salty water in-between is connected to the continental shelf through sloping isopycnals resulting from both Ekman pumping and dense water export. With the strong idealization of the model setup in mind, we will refer to these waters as Weddell Sea Bottom Water (WSBW) and Warm Deep Water (WDW). For a detailed discussion of the dynamical processes in the high-resolution setup, the reader is referred to Stewart and Thompson (2016).

At a resolution of 10 km, the isopycnal slopes are steeper as they cannot be relaxed as effectively in the absence of small-scale eddies (Fig. 2c-d). Consequently, the surface water is displaced further downward and pushes the WDW further offshore. As a result, both the shelf and the gravity current on the continental slope are colder. On the shelf, the isopycnals are now particularly steep and the salt input cannot be distributed as effectively in the horizontal. Close to the shelf break, interactions with the downward-displaced fresh surface water lead to an even fresher gravity current.

At such coarse resolution, the along-slope averaged eddy kinetic energy is orders of magnitude smaller compared to the high-resolution reference simulation (Fig. 3a-b). Similarly, the eddy component of the heat flux strongly reduces over the slope and shelf (Fig. 3c-d). In consequence, very little heat is moved offshore by the mean circulation. The salt fluxes are dominated by the mean component, which moves the salt injected over the shelf offshore, whereas the eddy component

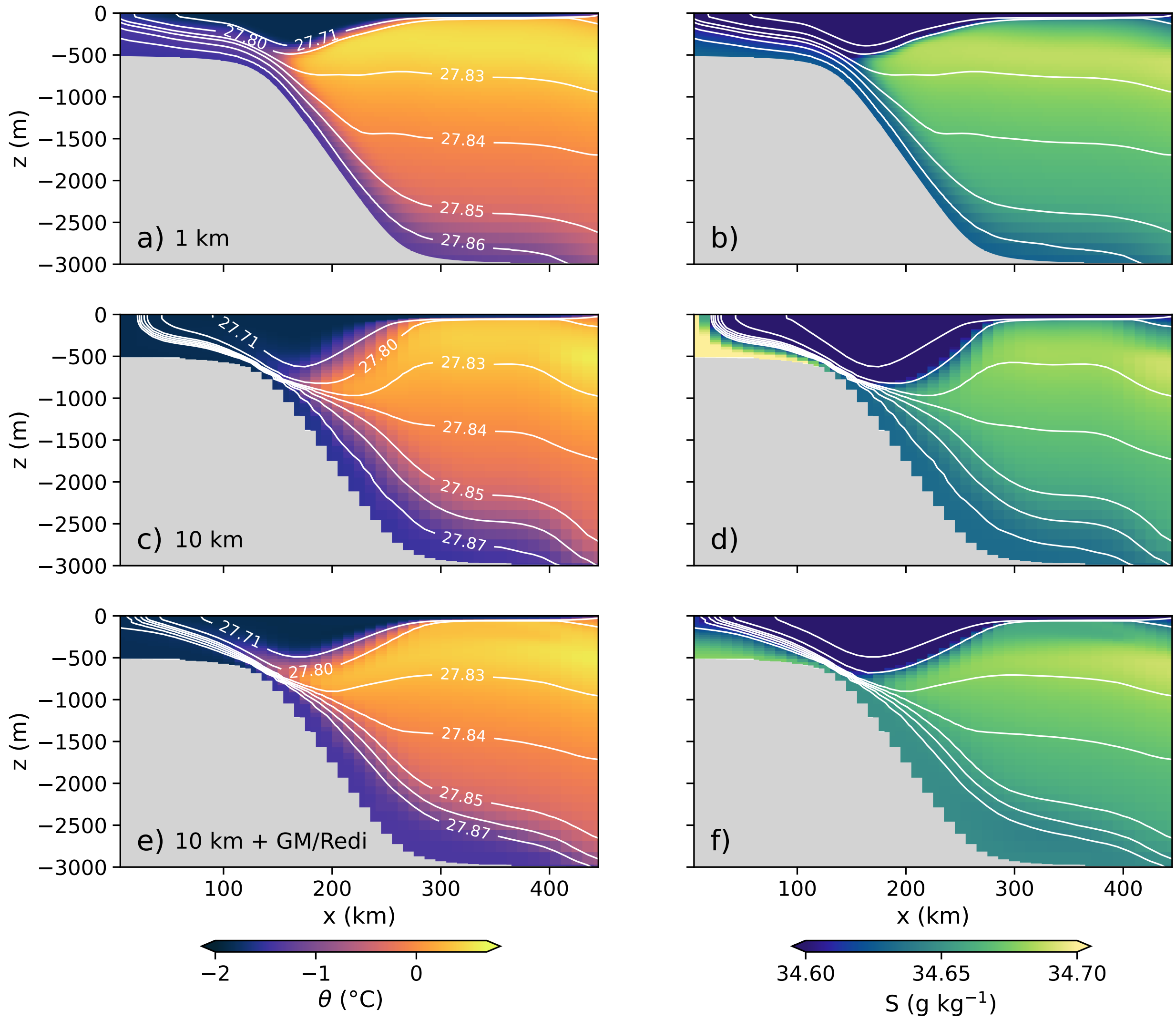


FIG. 2. Along-slope and time-averaged potential temperature (left column) and salinity (right column) for horizontal resolutions of 1 km (a, b) and 10 km without the GM/Redi scheme (c, d) and with the GM/Redi scheme setting $\kappa_{GM} = \kappa_{GM}^{diag}$ (e, f). The contour lines show the same selected levels of surface-referenced potential density in all panels.

of the salt flux is generally small (Fig. 3e-f). We therefore focus our discussion on the eddy heat fluxes.

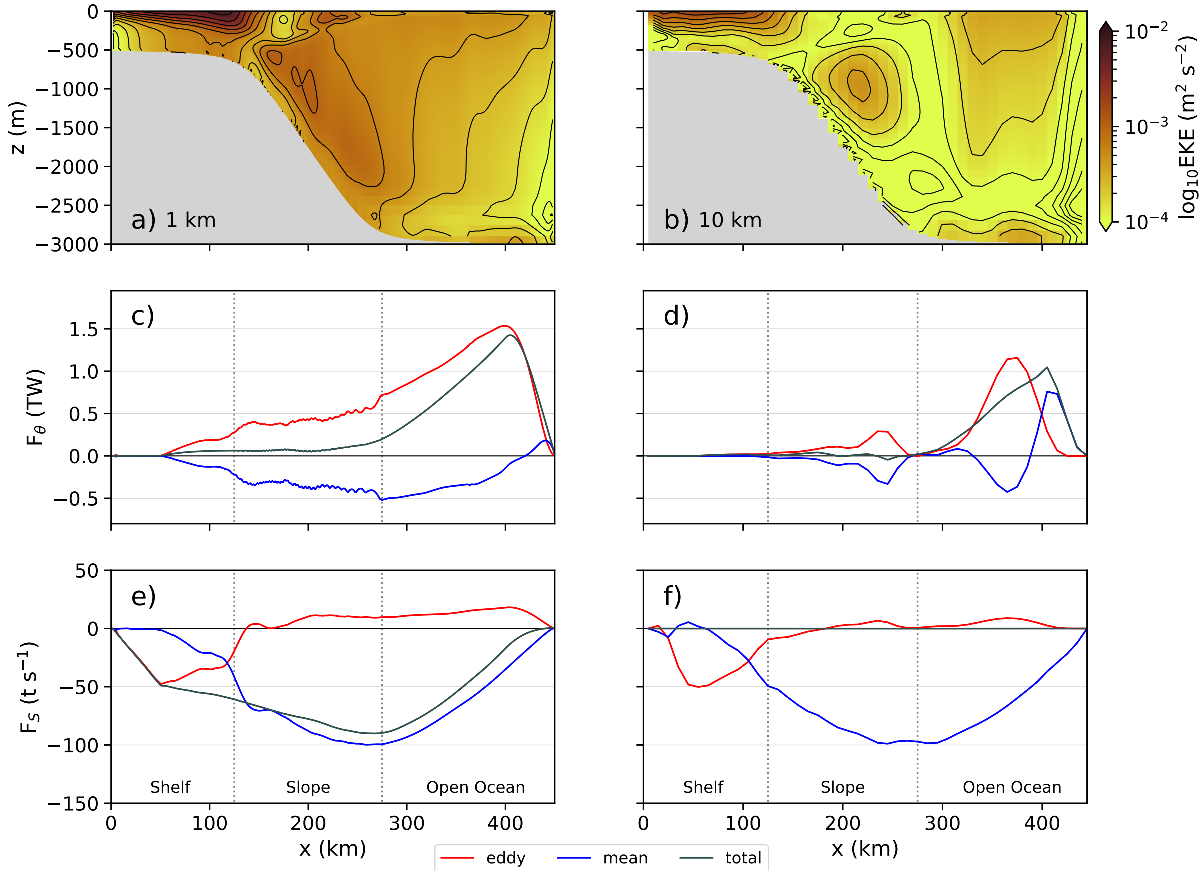


FIG. 3. Along-slope and time-averaged EKE (a, b, shading and contours), onshore heat (c, d) and salt (e, f) fluxes for horizontal resolutions of 1 km (left column) and 10 km (right column).

### *b. Estimating the GM diffusivity*

In section 3, we identified the strong underestimation of cross-slope heat transports and the differences in the mean isopycnal slopes as the main issues of the low-resolution simulation that an eddy parameterization needs to address. Now we test to which extent the GM/Redi parameterization can reproduce the effect of mesoscale eddies in this context and reduce the associated differences. For this, we need an initial estimate of the GM diffusivity. In the GM scheme, the bolus stream function is computed as the product of the GM diffusivity and the isopycnal slope (Eq. 1). With the "optimal" GM diffusivity, the resulting isopycnal slopes should match the isopycnal slopes in the high-resolution reference run. Additionally, the bolus stream function should then equal the eddy component of the overturning stream function $\psi_{eddy}$. We can thus obtain an estimate for the

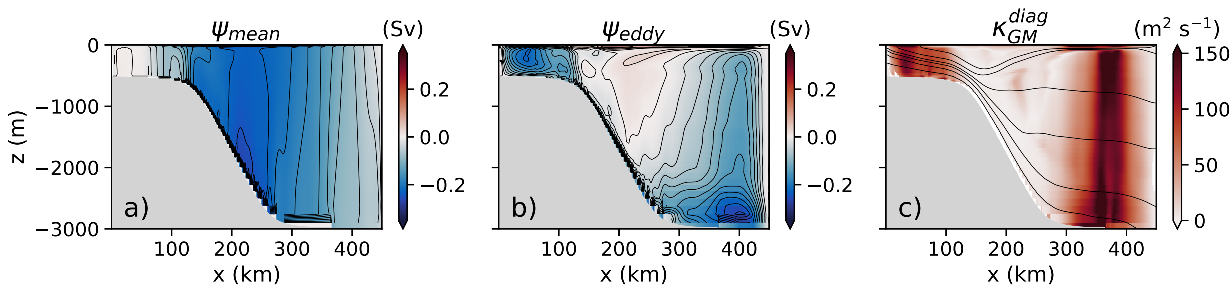


FIG. 4. Mean (a) and eddy (b) contributions to the residual overturning stream function (color shading and contours) and estimate of the GM diffusivity according to Eq. 19 (c). Contour lines in (c) show potential density (same levels as in Fig. 2).

GM diffusivity from Eq. 1:

$$\kappa_{GM}^{diag} = \frac{s_{iso,x}}{\psi_{eddy}}. \tag{19}$$

The main contribution to the transport across the slope at the depth of the WDW layer can be attributed to the eddy component of the overturning (Fig. 4). In contrast, mean cross-slope transports are confined to the surface and bottom. The estimated GM diffusivity $\kappa_{GM}^{diag}$ over the continental slope is strongly reduced by an order of magnitude compared to the shelf and open ocean (Fig. 4c). Noticeably, the diffusivities are very small directly over the continental slope where isopycnals are roughly parallel to the slope. At the AASW-WDW interface where the isopycnal and topographic slopes oppose each other, slightly higher diffusivities of $\mathcal{O}(15\,\mathrm{m^2\ s^{-1}})$ are observed, a value which is similar to observational estimates on the Weddell Sea continental slope (Thompson et al. 2014). This is consistent with theory and results of primitive equation simulations, where diffusivities are reduced in the presence of a sloping bottom, in particular where isopycnals are parallel to the topographic slope (Blumsack and Gierasch 1972; Isachsen 2011).

Analogous to other implementations of GM/Redi in MITgcm, we proceed by taking the vertical average of $\kappa_{GM}^{diag}$ as input for the GM scheme and compare the result to two choices of a constant $\kappa_{GM}$ approximately matching $\kappa_{GM}^{diag}$ over the continental slope ($\kappa_{GM}^{const,low} = 15\ \mathrm{m^2\ s^{-1}}$) and away from the slope ($\kappa_{GM}^{const,high} = 130\ \mathrm{m^2\ s^{-1}}$) (Fig. 5). Motivated by the strong damping of $\kappa_{GM}^{diag}$ over the slope, we also set up a simple "slope-aware" GM diffusivity. Note that we use the term "slope-aware" to refer to the dependency on the topographic slope since the GM scheme is - by design - already dependent on the isopycnal slope in its traditional form. Slope-aware diffusivity estimates $\kappa_{GM}^{slope}$ can be constructed by introducing a scaling factor $\Gamma$ that contains information about the topographic slope

$$\kappa_{GM}^{slope} = \Gamma \cdot \kappa_{GM}. \tag{20}$$

Here, we follow empirical scalings based on the slope Burger number $B_s$ and the topographic slope $s_{topo}$ (Brink 2012; Brink and Cherian 2013; Brink 2016; Wei and Wang 2021) of the form

$$\Gamma = \frac{1}{1 + \epsilon \cdot B_s}, \tag{21}$$

where $B_s = N \cdot \left|s_{topo}\right| / f_0$, $N$ is the buoyancy frequency and $\epsilon$ is a constant tuning factor. Since $f_0$ is constant in our model setup and the variations of $s_{topo}$ are 1-2 orders of magnitude larger than the variations in $N$ over the domain, we simplify so that

$$\kappa_{GM}^{slope} = \frac{1}{1 + \epsilon_c \cdot s_{topo}} \cdot \kappa_{GM}^{const,high}, \tag{22}$$

and set $\epsilon_c$ = 800 in order to reach an approximate agreement with $\kappa_{GM}^{diag}$. On the shelf and open ocean side, the topographic slope is small or zero so that the original diffusivity remains unchanged by $F$ whereas over the central slope, the GM diffusivity decreases by a factor of 10 very similar to the case of $\kappa_{GM}^{diag}$ (Fig. 5). In addition to prescribing the GM diffusivity, we use the scheme by Visbeck et al. (1997) with

$$\kappa_{GM}^{Vb97} = \alpha L^2 \overline{\frac{|f|}{\sqrt{Ri}}}^z. \tag{23}$$

Here, $\alpha$ is a constant factor, $L$ is a length scale, and $Ri = N^2/u_z^2$ is the Richardson number. Visbeck et al. (1997) find $\alpha = 0.015$ to be suitable for a wide range of applications for which we tune $L$ to obtain two diffusivity profiles that approximately match $\kappa_{GM}^{diag}$ over the slope or shelf and open ocean area respectively. The tuning results in values of $L_{high} = 40$ km and $L_{low} = 15$ km, which lie in the range of previously proposed length scales, namely the width of the baroclinic zone (Green 1970), the Rossby Radius of deformation (Stone 1972) or the model grid spacing (Kong and Jansen 2021). In both cases, the resulting GM diffusivity is higher over the shelf than over the slope since the Richardson number is lower over the shelf. Nevertheless, the damping over the continental

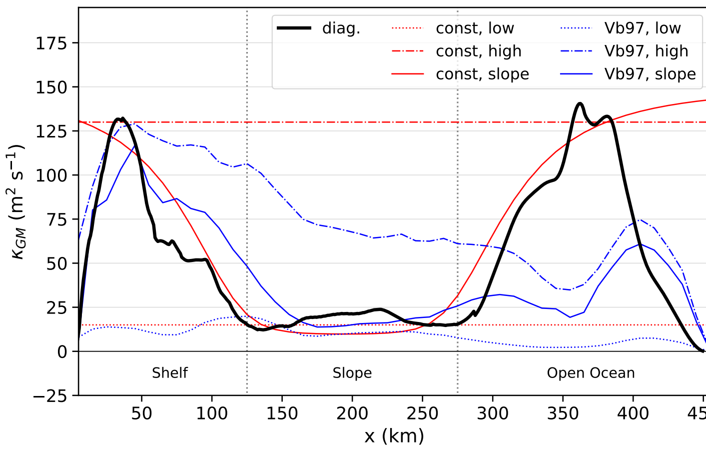


Fig. 5. Vertically averaged diffusivity $\kappa_{GM}^{diag}$ diagnosed from the high-resolution reference simulation according to Eq. 19 (black line), constant high and low GM diffusivities and slope-aware modification according to Eq. 22 (red lines), and high, low and slope-aware prognostic GM diffusivities (Visbeck et al. 1997) according to Eq. 23, 24 (blue lines). See main text for further details.

slope is still much smaller than for $\kappa_{GM}^{diag}$. This is why we implement a slope-aware version of the Visbeck scheme analogous to Eq. 22 of the form

$$\kappa_{GM}^{Vb97,slope} = \frac{1}{1+\epsilon_{Vb97}\cdot s_{topo}} \cdot \kappa_{GM}^{Vb97,high}. \tag{24}$$

When choosing $\epsilon_{Vb97} = 175$, Eq. 24 yields a GM diffusivity similar to the diagnosed $\kappa_{GM}^{diag}$ (Fig. 5).

We proceed by first evaluating the performance of the parameterization using $\kappa_{GM}$=$\kappa_{GM}^{diag}$ representing the "best estimate" of the transfer coefficient. We then discuss the results obtained using constant values for $\kappa_{GM}$, prognostic diffusivities produced by the Visbeck et al. (1997) scheme and their respective slope-aware version (Eq. 22, 24). For all simulations, we choose a spatially uniform isopycnal diffusivity of $\kappa_{Redi}$ = 15 m s$^{-2}$. The choice of $\kappa_{Redi}$ is the result of tuning; a detailed investigation of the effect of the Redi scheme in this context is beyond the scope of this work.

*c. Using the diagnosed GM diffusivity to parameterize shoreward heat fluxes*

With the GM/Redi parameterization isopycnal slopes relax, particularly at the AASW-WDW interface (Fig. 2, e-f). The V-shaped isopycnals move upward, lifting the layer of warm and salty WDW by around 200 m. WDW is found further onshore where it can reach the shelf break. This also affects the deep water exported within the gravity current, which becomes slightly warmer with GM/Redi. Over the continental shelf, the flattened isopycnals reduce the accumulation of salt and thus the salinity error locally. Nevertheless, the vertical exchange with the fresh surface water is underestimated so that the gravity current is slightly too salty.

In total, the domain integrated root mean square differences computed between the coarse resolution and the coarse-grained high-resolution fields reduce by 58.7% for temperature and 44.6% for salinity with the GM/Redi scheme. We conclude that the eddy parameterization generally improves the hydrographic structure in this application although some differences persist. In particular, the gravity current on the continental slope remains too broad whereas it is strongly confined to the slope at high resolution. This is a well-known phenomenon in $z$-coordinate ocean models where the down-slope transport of dense water is subject to excessive entrainment unless $\Delta x < \Delta z/\alpha$ (Winton et al. 1998). Considering a vertical grid spacing of $\Delta z = 75$ m at the center of the slope and a topographic slope of $s_{topo} = 0.02$, the "slope-resolving" horizontal resolution $\Delta z/s_{topo} = 3.75$ km is only reached in the high-resolution reference simulation. Therefore, we cannot expect the eddy parameterization to resolve this issue.

In the simulation with the GM/Redi parameterization, the shoreward heat flux is considerably larger over most of the domain (Fig. 6a). Mainly, the GM scheme produces a strong heat flux over the central continental slope and in the open ocean area, which is very similar to the high-resolution simulation. This is consistent with the bolus stream function $\psi_{bolus}$, which generally compares favorably to the computed eddy stream function $\psi_{eddy}$ (Fig. 6b). Here, the positive vertical gradient of $\psi_{bolus}$ generates a shoreward bolus velocity in the WDW layer according to Eq. 2. Approaching the shelf break, the vertical gradient of the bolus stream function reduces and the cross-slope heat flux becomes small. We conclude that because of the shape and polarity of the bolus stream function, no substantial shoreward heat flux can be achieved with the GM scheme independent of the choice of the GM coefficient. On the upper slope, the Redi scheme takes over and captures some of the shoreward heat flux across the shelf break, even though these heat fluxes are about 50%

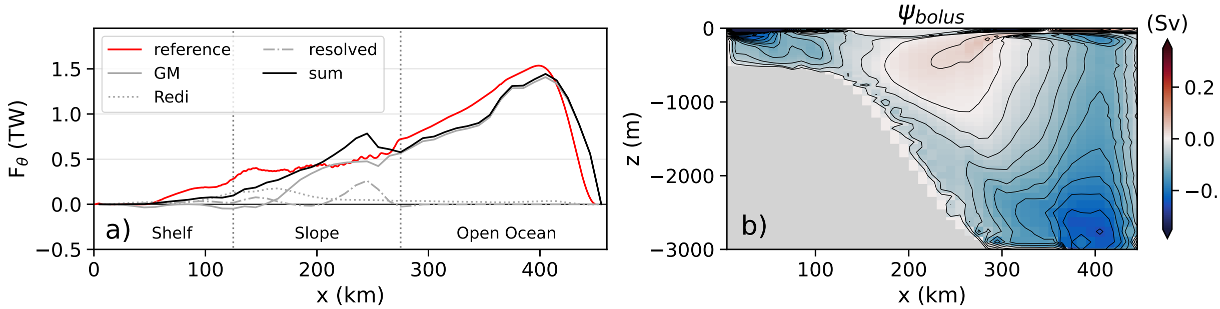


FIG. 6. Onshore heat fluxes decomposed into the contributions of the GM scheme, the Redi scheme and the resolved eddies for a horizontal resolution of 10 km using GM/Redi with vertically averaged $\kappa_{GM}^{diag}$ and $\kappa_{Redi}$=15 m$^2$ s$^{-1}$ compared to the eddy heat flux of the high-resolution reference simulation (a). Along-slope and time-averaged bolus stream function $\psi_{bolus}$ (b).

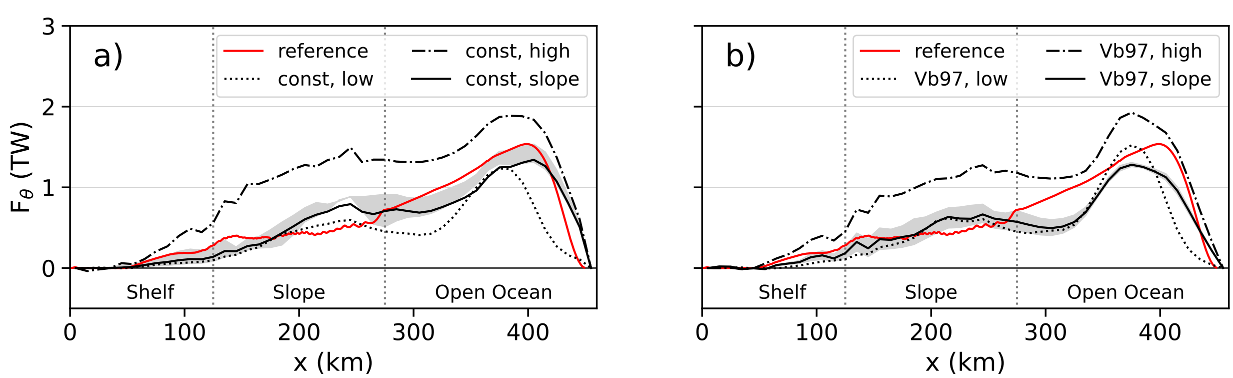


FIG. 7. Along-slope and time averaged onshore eddy heat flux at 1 km resolution and onshore heat flux at 10 km resolution using the GM/Redi scheme with $\kappa_{GM}^{const}$ (a) and $\kappa_{GM}^{Vb97}$ (b). The black curves represent the sum of heat fluxes from the GM/Redi scheme and from resolved eddies. The GM diffusivities (high, low, slope) are the same as in Fig. 5. The grey envelope shows the area between solutions obtained by doubling and halving the value of the tuning parameters $\epsilon_c$ and $\epsilon_{Vb97}$ of the "slope-aware" modification to the GM scheme (Eq. 22, 24).

smaller than in the high-resolution reference. Some improvements to the heat fluxes over the shelf can be achieved by locally setting a higher $\kappa_{Redi}$ but this resulted in overly strong diffusion at the AASW-WDW interface (not shown). A detailed investigation of how to set $\kappa_{Redi}$ is an important task for future work, especially for the modeling of ocean-ice shelf interactions which requires the correct amount of heat to be transported onto the shelf.

*d. Slope-aware GM coefficients*

With a properly designed diffusivity, an idealized model of the Weddell Sea continental slope with the GM scheme shows improved cross-slope heat fluxes and hydrographic mean state. An appropriate diffusivity informed by a high-resolution reference simulation, however, is usually not available beforehand. Instead, a modeler usually chooses a constant value for the GM diffusivity or employs a flow-dependent scheme (e.g. Visbeck et al. 1997). Neither solution takes into account the suppressive effect of the continental slope as shown in Fig. 5.

We now contrast the results obtained with and without the slope-aware versions of the GM scheme (Eq. 22, 24). With a high prescribed or prognostic diffusivity appropriate for shelf or open ocean, the onshore heat fluxes are strongly overestimated (Figure 7, dash-dotted lines). This is because WDW can directly access the continental shelf and erode the V-shaped isopycnal structure of the ASF, once the suppressive influence of the topographic slope is neglected (Fig. 8). Choosing a diffusivity appropriate only for the continental slope instead, the onshore heat flux is underestimated at the transition from the slope to the open ocean (Figure 7, dotted lines). Moreover, the isopycnal slopes over the continental shelf become too steep, which again leads to an accumulation of salt similar to the coarse resolution simulation without the GM/Redi parameterization (not shown). Also, the low diffusivity choice is less realistic since a diffusivity suitable for the open ocean would most likely be given preference in a larger model domain.

The slope-aware version of the GM scheme yields both reasonable heat fluxes across the continental slope and improvements to the isopycnal slopes on the shelf. Further, the heat fluxes do not depend very much on the choice of the slope parameter $\epsilon_c$ or $\epsilon_{Vb97}$ (Fig. 7, grey envelope). The slope-aware modification to the GM scheme thus seems to perform fairly robustly in the given application.

Some differences between using a prescribed or prognostic diffusivity are apparent on the open ocean side of the domain. We note that the model resolves some eddies here, which are damped in cases with high offshore GM diffusivity. The damping of resolved eddies could have been avoided by choosing an even coarser resolution, which would however have resulted in fewer grid points over the slope leading to an even less realistic representation of the gravity current. Since we expect the sponge layer also to influence the open ocean side, we refrain from further interpreting these differences and discuss the implications of the interaction of GM and resolved eddies in section 4.

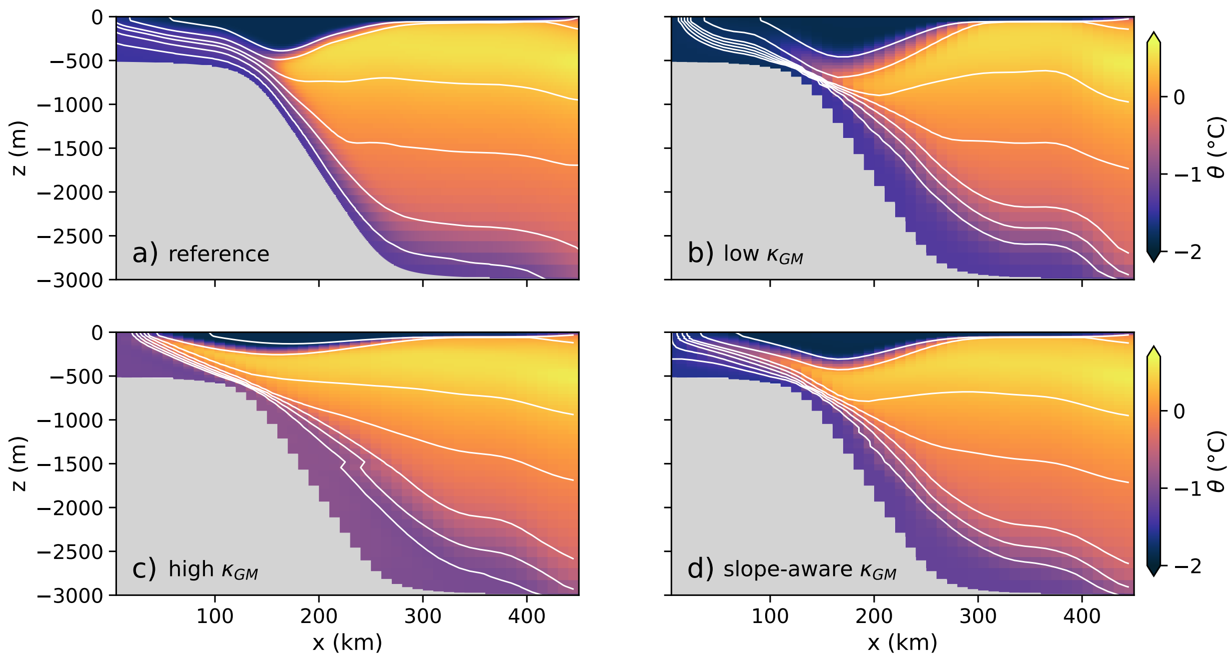


FIG. 8. Along-slope and time averaged potential temperature at horizontal resolution 1 km (a) and 10 km using GM/Redi with $\kappa_{GM}^{Vb97,low}$ (b), $\kappa_{GM}^{Vb97,high}$ (c) and $\kappa_{GM}^{Vb97,slope}$ (d). The GM diffusivities (high, low, slope) are the same as in Fig. 5.

In summary, the GM/Redi scheme improves the coarse resolution simulation in every aspect that we have investigated (Fig. 9). In particular, the largest improvements are observed for the mean hydrographic fields and cross-slope heat fluxes where the root mean square differences to the high-resolution reference simulation reduce by half compared to the simulation without GM/Redi. While the effect on the total velocity of the ASC is small, the baroclinic component also improves considerably as the isopycnal slopes are relaxed by the parameterization.

Making the GM coefficient depend on the topographic slope reduces the differences to the high-resolution reference simulation as much as using a diagnosed GM diffusivity. Most importantly, the slope-aware versions of the parameterization generally outperform the traditional versions and seem insensitive to details of the new tuning parameter $\epsilon$. We conclude, that a carefully chosen, small GM diffusivity over the continental slope is essential to simulating correct cross-slope heat fluxes. Using a diffusivity value in the traditional GM scheme that is derived from open ocean simulation will not yield a small coefficient but will lead to too large cross-slope heat fluxes. Only

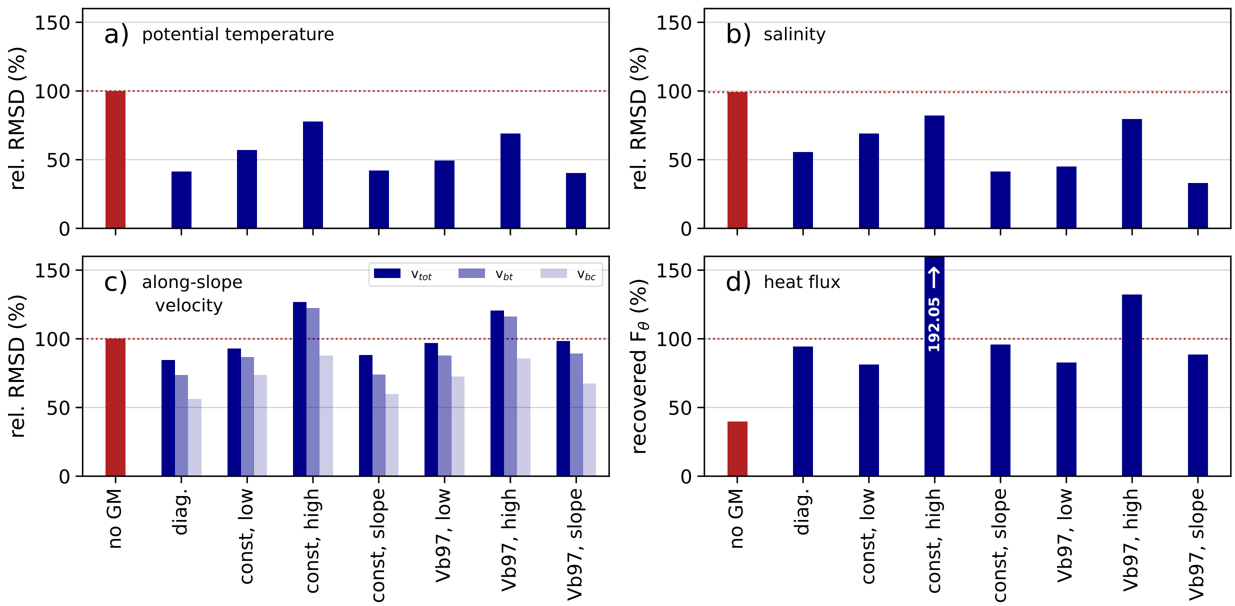


FIG. 9. Volume weighted root mean square difference (RMSD) of potential temperature (a), salinity (b), and barotropic, baroclinic and total along-slope velocities $v_{bt}$, $v_{bc}$ and $v_{tot}$ between the coarse-grained high-resolution simulation and the coarse-resolution simulation with different $\kappa_{GM}$. Bars show relative RMSD compared to the simulation without the GM/Redi scheme. Panel (d) shows integrated cross-slope heat fluxes (sum of contributions from GM/Redi scheme and resolved eddies) relative to the integrated cross-slope eddy heat flux of the high-resolution simulation (d). All integrals are computed for the complete model domain excluding the sponge layer.

with a slope-aware version of the GM scheme the prescribed and prognostic GM diffusivities match the diagnosed diffusivity for both the continental slope and the shelf and open ocean parts of the model domain and more realistic simulations are possible.

## 4. Summary and discussion

In this work, we assess the effect of the GM/Redi parameterization for mesoscale eddies in an idealized model of the Weddell Sea continental shelf and slope. We find that with the GM/Redi scheme, WDW is generally moved towards the continental shelf and a heat flux comparable to a high-resolution reference is simulated. Here, the GM scheme transfers WDW across the central continental slope whereas the Redi scheme generates a diffusive heat flux across the continental shelf break. As the main result, a successful simulation with the GM/Redi parameterization crucially depends on a choice of the GM diffusivity that reflects the suppressive effect of the continental slope where in this application the diffusivity is reduced by an order of magnitude. Schemes designed for the open ocean that diagnose $\kappa_{GM}$ only from the resolved flow - represented here by the Visbeck et al. (1997) scheme - cannot capture this behavior and instead yield a fairly constant thickness diffusivity. Neglecting the attenuation of the eddy diffusivity over the continental slope here results in a strong overestimation of onshore WDW transport or in a misrepresentation of shelf and open ocean hydrographic mean states.

Our experiments illustrate clearly the limitation of the GM parameterization in the presence of topographic slopes and highlight how important "slope-aware" eddy parameterizations may become, in which the GM diffusivity is also a function of the topographic slope. In idealized simulations with both $\delta < 0$ and $\delta > 0$, the diagnostic scaling of cross-slope eddy buoyancy fluxes improves when it is a function of the slope Burger number or the slope (Wei et al. 2022; Wang and Stewart 2020). In the next step, these diagnostic scalings need to be implemented as an estimate of the eddy diffusivity in regional to global ocean models to assess whether they also improve the representation of buoyancy fluxes in flow regimes such as the ASC. A good starting point could be to modify diagnostic schemes that already include aspects of the dynamic flow (e.g. Visbeck et al. 1997), where the computation of $\kappa_{GM}$ can be easily adjusted. More complicated schemes that integrate a prognostic subgrid eddy kinetic energy equation (Eden and Greatbatch 2008; Marshall et al. 2012; Mak et al. 2018) may require more substantial modifications.

As computing power increases, global ocean models will (at least partially) resolve mesoscale eddies in the open ocean while smaller eddies on the slope remain unresolved. Various techniques have been proposed to limit the damping effect of GM onto the resolved eddies, including scaling

$\kappa_{GM}$ by the first baroclinic deformation radius and the horizontal grid spacing (Hallberg 2013) or a splitting approach where GM only acts on the large-scale field (Mak et al. 2023).

In our configuration, the Redi scheme produces an onshore diffusive heat flux. The choice of $\kappa_{Redi}$, however, is the result of tuning and not backed by dynamical considerations. For a flat bottom, $\kappa_{Redi}$ may be inferred from $\kappa_{GM}$ (Abernathey et al. 2013), but the derived relationship remains untested for continental slopes. A $\kappa_{Redi}$ that is a function of the topographic slope may enhance the performance of the Redi scheme over continental slopes (Wei and Wang 2021). We conclude that the behavior of the Redi scheme and its interaction with the GM scheme in the context of the ASF raises questions to be answered in future work.

The idealized model setup carries some limitations. First of all, we do not consider topographic variations in the along-slope direction that can influence both the intensity and distribution of cross-slope buoyancy fluxes. Around the Antarctic continental margin, dense water export and associated eddy-driven shoreward heat fluxes concentrate in bathymetric depressions (e.g. Orsi and Wiederwohl 2009; Williams et al. 2010; Stewart et al. 2018; Morrison et al. 2020; Stewart 2021). Additionally, along-slope topographic features act as drivers of buoyancy transfers across continental slopes through the generation of standing eddies (e.g. Abernathey and Cessi 2014; St-Laurent et al. 2013; Bai et al. 2021; Si et al. 2022). Even when along-slope topographic variations are present, we may still expect the presented topographic scaling to lead to improvements since transient eddy fluxes have been shown to dominate over standing eddy fluxes across slope currents such as the ASC (Wei et al. 2022; Si et al. 2022). Also, diagnostic scalings of eddy buoyancy fluxes across idealized slope fronts tuned over smooth topography still outperform traditional schemes when applied to cases in which the topography varies along the slope (Wang and Stewart 2020; Wei et al. 2022). Furthermore, the idealized model neglects the variability in the wind forcing and associated impacts on the outflow of dense water from the ice shelf cavities in the Weddell Sea (Wang et al. 2012; Daae et al. 2018) and the inflow of warm water into the cavities through modification of coastal currents (Hellmer et al. 2012; Darelius et al. 2016). Moreover, we do not account for the effect of tides, which contribute to setting up the structure of the ASF through tidal rectification (Flexas et al. 2015), shape heat fluxes across the ASF (Stewart et al. 2018; Stewart 2021; Si et al. 2022, 2023) and drive an onshore residual flow of CDW (Wang et al. 2013). While considering the thermodynamic effects of sea ice, we also do not account for the influence of sea ice dynamics on the transfer of momentum between atmosphere and ocean (Si et al. 2022). Finally, the lack of an ice shelf cavity in the idealized configuration excludes processes that form dense water such as the transformation of HSSW into ISW through the input of meltwater under the ice shelf (Hattermann et al. 2012). Reducing the degree of idealization by adding an ice shelf cavity would allow tracking the influence of the parameterization on the melting of ice shelves and the sources of dense water and could therefore serve as an intermediate step on the way to regional and global modeling.

The central role of the Weddell Sea in producing bottom water and thereby shaping the global ocean circulation requires an accurate estimation of heat transports across the Weddell Sea continental slope. In light of the strong signs of anthropogenic climate change around the Antarctic continental margin, a skillful representation of eddy feedback mechanisms that moderate the exchange between shelf and open ocean (Si et al. 2023) is particularly necessary. Our application and improvement of existing parameterizations represent an important step towards improving heat transports across the Weddell Sea continental slope in non-eddy-resolving and eddy-permitting ocean models.

*Acknowledgments.* This paper is a contribution to the project T3 (Energy Transfers in Gravity Currents) of the Collaborative Research Centre TRR 181 “Energy Transfers in Atmosphere and Ocean” funded by the Deutsche Forschungsgemeinschaft (DFG, German Research Foundation, project number 274762653). We thank Andrew Stewart for providing configuration files for the MITgcm reference simulation.

*Data availability statement.* The MITgcm code can be accessed at `https://github.com/MITgcm` and documentation is provided at `https://mitgcm.readthedocs.io/en/latest`. Modifications to the model code required to reproduce the simulations are available at `https://github.com/nicolasdettling/weddell_gm.git`. Once accepted the final code modifications will be published on Zenodo. Input files and namelists to rerun all experiments are stored at `https://doi.org/10.5281/zenodo.10033249`.

## References

Abernathey, R., and P. Cessi, 2014: Topographic enhancement of eddy efficiency in baroclinic equilibration. *Journal of Physical Oceanography*, **44 (8)**, 2107 – 2126, https://doi.org/10.1175/JPO-D-14-0014.1.

Abernathey, R., D. Ferreira, and A. Klocker, 2013: Diagnostics of isopycnal mixing in a circumpolar channel. *Ocean Modelling*, **72**, 1–16, https://doi.org/10.1016/j.ocemod.2013.07.004.

Abernathey, R., J. Marshall, and D. Ferreira, 2011: The dependence of Southern Ocean meridional overturning on wind stress. *Journal of Physical Oceanography*, **41 (12)**, 2261 – 2278, https://doi.org/10.1175/JPO-D-11-023.1.

Bai, Y., Y. Wang, and A. L. Stewart, 2021: Does topographic form stress impede prograde ocean currents? *Journal of Physical Oceanography*, **51 (8)**, 2617 – 2638, https://doi.org/10.1175/JPO-D-20-0189.1.

Blumsack, S. L., and P. J. Gierasch, 1972: Mars: The effects of topography on baroclinic instability. *Journal of Atmospheric Sciences*, **29 (6)**, 1081 – 1089, https://doi.org/10.1175/1520-0469(1972)029⟨1081:MTEOTO⟩2.0.CO;2.

Brink, K., 2012: Baroclinic instability of an idealized tidal mixing front. *Journal of Marine Research*, **70**, https://doi.org/10.1357/002224012805262716.

Brink, K. H., 2016: Continental shelf baroclinic instability. part I: Relaxation from upwelling or downwelling. *Journal of Physical Oceanography*, **46 (2)**, 551 – 568, https://doi.org/10.1175/JPO-D-15-0047.1.

Brink, K. H., and D. A. Cherian, 2013: Instability of an idealized tidal mixing front: Symmetric instabilities and frictional effects. *Journal of Marine Research*, **71 (6)**, 425–450, https://doi.org/doi:10.1357/002224013812587582.

Bronselaer, B., M. Winton, S. M. Griffies, W. J. Hurlin, K. B. Rodgers, O. V. Sergienko, R. J. Stouffer, and J. L. Russell, 2018: Change in future climate due to Antarctic meltwater. *Nature*, **564**, 53–58, https://doi.org/10.1038/s41586-018-0776-9.

Cessi, P., 2008: An energy-constrained parameterization of eddy buoyancy flux. *Journal of Physical Oceanography*, **38 (8)**, 1807 – 1819, https://doi.org/10.1175/2007JPO3812.1.

Cook, A. J., A. J. Fox, D. G. Vaughan, and J. G. Ferrigno, 2005: Retreating glacier fronts on the Antarctic Peninsula over the past half-century. *Science*, **308 (5721)**, 541–544, https://doi.org/10.1126/science.1104235.

Daae, K., E. Darelius, I. Fer, S. Østerhus, and S. Ryan, 2018: Wind stress mediated variability of the Filchner Trough overflow, Weddell Sea. *Journal of Geophysical Research: Oceans*, **123 (5)**, 3186–3203, https://doi.org/10.1002/2017JC013579.

Daae, K., T. Hattermann, E. Darelius, and I. Fer, 2017: On the effect of topography and wind on warm water inflow—an idealized study of the southern Weddell Sea continental shelf system. *Journal of Geophysical Research: Oceans*, **122 (3)**, 2622–2641, https://doi.org/10.1002/2016JC012541.

Darelius, E., I. Fer, and K. W. Nicholls, 2016: Observed vulnerability of Filchner-Ronne Ice Shelf to wind-driven inflow of warm deep water. *Nature Communications*, **7**, https://doi.org/10.1038/ncomms12300.

Darelius, E., and Coauthors, 2023: Observational evidence for on-shelf heat transport driven by dense water export in the Weddell Sea. *Nature Communications*, **14**, 1022, https://doi.org/10.1038/s41467-023-29234-5.

DeConto, R. M., and D. Pollard, 2016: Contribution of Antarctica to past and future sea-level rise. *Nature*, **531 (7596)**, 591–597, https://doi.org/10.1038/nature17145.

Döös, K., and D. J. Webb, 1994: The Deacon Cell and the other meridional cells of the Southern Ocean. *Journal of Physical Oceanography*, **24 (2)**, 429 – 442, https://doi.org/10.1175/1520-0485(1994)024⟨0429:TDCATO⟩2.0.CO;2.

Eden, C., and R. J. Greatbatch, 2008: Towards a mesoscale eddy closure. *Ocean Modelling*, **20**, 223–239, https://doi.org/10.1016/j.ocemod.2007.09.002.

Fahrbach, E., G. Rohardt, N. Scheele, M. Schroder, V. Strass, and A. Wisotzki, 1995: Formation and discharge of deep and bottom water in the northwestern Weddell Sea. *Journal of Marine Research*, **53**, 515–538, https://doi.org/10.1357/0022240953213089.

Flexas, M. M., M. P. Schodlok, L. Padman, D. Menemenlis, and A. H. Orsi, 2015: Role of tides on the formation of the Antarctic Slope Front at the Weddell-Scotia Confluence. *Journal of Geophysical Research: Oceans*, **120 (5)**, 3658–3680, https://doi.org/10.1002/2014JC010372.

Foldvik, A., and Coauthors, 2004: Ice shelf water overflow and bottom water formation in the southern Weddell Sea. *Journal of Geophysical Research: Oceans*, **109 (C2)**, https://doi.org/10.1029/2003JC002008.

Fox-Kemper, B., and R. Ferrari, 2008: Parameterization of mixed layer eddies. part II: Prognosis and impact. *Journal of Physical Oceanography*, **38 (6)**, 1166 – 1179, https://doi.org/10.1175/2007JPO3788.1.

Gent, P. R., and J. C. McWilliams, 1990: Isopycnal mixing in ocean circulation models. *Journal of Physical Oceanography*, **20 (1)**, 150 – 155, https://doi.org/10.1175/1520-0485(1990)020⟨0150:IMIOCM⟩2.0.CO;2.

Gerdes, R., C. Köberle, and J. Willebrand, 1991: The influence of numerical advection schemes on the results of ocean general circulation models. *Climate Dynamics*, **5 (4)**, 211–226, https://doi.org/10.1007/BF00210006.

Gill, A. E., 1973: Circulation and bottom water production in the Weddell Sea. *Deep Sea Research and Oceanographic Abstracts*, **20 (2)**, 111–140, https://doi.org/10.1016/0011-7471(73)90048-X.

Gordon, A. L., M. Visbeck, and B. Huber, 2001: Export of Weddell Sea deep and bottom water. *Journal of Geophysical Research: Oceans*, **106 (C5)**, 9005–9017, https://doi.org/10.1029/2000JC000281.

Green, J. S. A., 1970: Transfer properties of the large-scale eddies and the general circulation of the atmosphere. *Quarterly Journal of the Royal Meteorological Society*, **96 (408)**, 157–185, https://doi.org/10.1002/qj.49709640802.

Hallberg, R., 2013: Using a resolution function to regulate parameterizations of oceanic mesoscale eddy effects. *Ocean Modelling*, **72**, 92–103, https://doi.org/10.1016/j.ocemod.2013.08.007.

Hallberg, R., and A. Gnanadesikan, 2006: The role of eddies in determining the structure and response of the wind-driven southern hemisphere overturning: Results from the modeling eddies in the Southern Ocean (meso) project. *Journal of Physical Oceanography*, **36 (12)**, 2232 – 2252, https://doi.org/10.1175/JPO2980.1.

Hattermann, T., O. A. Nst, J. M. Lilly, and L. H. Smedsrud, 2012: Two years of oceanic observations below the Fimbul Ice Shelf, Antarctica. *Geophysical Research Letters*, **39 (12)**, https://doi.org/10.1029/2012GL051012.

Hellmer, H. H., F. Kauker, R. Timmermann, J. Determann, and J. Rae, 2012: Twenty-first-century warming of a large Antarctic ice-shelf cavity by a redirected coastal current. *Nature*, **485**, 225–228, https://doi.org/10.1038/nature11064.

Isachsen, P. E., 2011: Baroclinic instability and eddy tracer transport across sloping bottom topography: How well does a modified Eady model do in primitive equation simulations? *Ocean Modelling*, **39 (1)**, 183–199, https://doi.org/10.1016/j.ocemod.2010.09.007.

Jacobs, S. S., 1991: On the nature and significance of the Antarctic Slope Front. *Marine Chemistry*, **35 (1)**, 9–24, https://doi.org/10.1016/S0304-4203(09)90005-6.

Jacobs, S. S., H. Hellmer, C. S. M. Doake, A. Jenkins, and R. Frolich, 1992: Melting of ice shelves and the mass balance of Antarctica. *Journal of Glaciology*, **38 (130)**, 375–387.

Janout, M. A., and Coauthors, 2021: FRIS revisited in 2018: On the circulation and water masses at the Filchner and Ronne Ice Shelves in the southern Weddell Sea. *Journal of Geo-*

*physical Research: Oceans*, **126 (6)**, e2021JC017 269, https://doi.org/https://doi.org/10.1029/2021JC017269.

Jansen, M. F., A. J. Adcroft, R. Hallberg, and I. M. Held, 2015: Parameterization of eddy fluxes based on a mesoscale energy budget. *Ocean Modelling*, **92**, 28–41, https://doi.org/10.1016/j.ocemod.2015.05.007.

Jenkins, A., and C. S. M. Doake, 1991: Ice-ocean interaction on Ronne Ice Shelf, Antarctica. *Journal of Geophysical Research: Oceans*, **96 (C1)**, 791–813, https://doi.org/10.1029/90JC01952.

Joughin, I., D. Shapero, B. Smith, P. Dutrieux, and M. Barham, 2021: Ice-shelf retreat drives recent Pine Island Glacier speedup. *Science Advances*, **7 (24)**, eabg3080, https://doi.org/10.1126/sciadv.abg3080.

Joughin, I., B. E. Smith, and B. Medley, 2014: Marine ice sheet collapse potentially under way for the Thwaites Glacier Basin, West Antarctica. *Science*, **344 (6185)**, 735–738, https://doi.org/10.1126/science.1249055.

Kong, H., and M. F. Jansen, 2021: The impact of topography and eddy parameterization on the simulated Southern Ocean circulation response to changes in surface wind stress. *Journal of Physical Oceanography*, **51 (3)**, 825 – 843, https://doi.org/10.1175/JPO-D-20-0142.1.

Large, W. G., J. C. McWilliams, and S. C. Doney, 1994: Oceanic vertical mixing: A review and a model with a nonlocal boundary layer parameterization. *Reviews of Geophysics*, **32 (4)**, 363–403, https://doi.org/10.1029/94RG01872.

Le Paih, N., T. Hattermann, O. Boebel, T. Kanzow, C. Lüpkes, G. Rohardt, V. Strass, and S. Herbette, 2020: Coherent seasonal acceleration of the Weddell Sea boundary current system driven by upstream winds. *Journal of Geophysical Research: Oceans*, **125 (10)**, e2020JC016 316, https://doi.org/https://doi.org/10.1029/2020JC016316.

Mak, J., J. R. Maddison, D. P. Marshall, and D. R. Munday, 2018: Implementation of a geometrically informed and energetically constrained mesoscale eddy parameterization in an ocean circulation model. *Journal of Physical Oceanography*, **48 (10)**, 2363 – 2382, https://doi.org/10.1175/JPO-D-18-0017.1.

Mak, J., J. R. Maddison, D. P. Marshall, X. Ruan, Y. Wang, and L. Yeow, 2023: Scale-awareness in an eddy energy constrained mesoscale eddy parameterization. 2306.08988.

Marshall, D. P., J. R. Maddison, and P. S. Berloff, 2012: A framework for parameterizing eddy potential vorticity fluxes. *Journal of Physical Oceanography*, **42 (4)**, 539–557, https://doi.org/10.1175/JPO-D-11-048.1.

Marshall, J., A. Adcroft, C. Hill, L. Perelman, and C. Heisey, 1997: A finite-volume, incompressible Navier Stokes model for studies of the ocean on parallel computers. *Journal of Geophysical Research: Oceans*, **102 (C3)**, 5753–5766, https://doi.org/10.1029/96JC02775.

McDougall, T. J., D. R. Jackett, D. G. Wright, and R. Feistel, 2003: Accurate and computationally efficient algorithms for potential temperature and density of seawater. *Journal of Atmospheric and Oceanic Technology*, **20 (5)**, 730 – 741, https://doi.org/10.1175/1520-0426(2003)20⟨730:AACEAF⟩2.0.CO;2.

McIntosh, P. C., and T. J. McDougall, 1996: Isopycnal averaging and the residual mean circulation. *Journal of Physical Oceanography*, **26 (8)**, 1655 – 1660, https://doi.org/10.1175/1520-0485(1996)026⟨1655:IAATRM⟩2.0.CO;2.

Mechoso, C. R., 1980: Baroclinic instability of flows along sloping boundaries. *Journal of Atmospheric Sciences*, **37 (6)**, 1393 – 1399, https://doi.org/10.1175/1520-0469(1980)037⟨1393:BIOFAS⟩2.0.CO;2.

MITgcm Group, 2023: user manual. Last accessed: 2023-10-02, https://mitgcm.readthedocs.io/en/latest/.

Morrison, A. K., A. M. Hogg, M. H. England, and P. Spence, 2020: Warm circumpolar deep water transport toward Antarctica driven by local dense water export in canyons. *Science Advances*, **6 (18)**, eaav2516, https://doi.org/10.1126/sciadv.aav2516.

Nicholls, K. W., S. Østerhus, K. Makinson, T. Gammelsrød, and E. Fahrbach, 2009: Ice-ocean processes over the continental shelf of the southern Weddell Sea, Antarctica: A review. *Reviews of Geophysics*, **47**, RG3003, https://doi.org/10.1029/2007RG000250.

Nicholls, K. W., S. Østerhus, K. Makinson, and M. R. Johnson, 2001: Oceanographic conditions south of Berkner Island, beneath Filchner-Ronne Ice Shelf, Antarctica. *Journal of Geophysical Research: Oceans*, **106 (C6)**, 11 481–11 492, https://doi.org/https://doi.org/10.1029/2000JC000350.

Orsi, A., G. Johnson, and J. Bullister, 1999: Circulation, mixing, and production of Antarctic Bottom Water. *Progress in Oceanography*, **43 (1)**, 55–109, https://doi.org/10.1016/S0079-6611(99)00004-X.

Orsi, A. H., and T. Whitworth III, 2005: *Hydrographic Atlas of the World Ocean Circulation Experiment (WOCE), vol. 1, Southern Ocean*. International World Ocean Circulation Experiment Project Office, Southampton, UK.

Orsi, A. H., and C. L. Wiederwohl, 2009: A recount of Ross Sea waters. *Deep Sea Research Part II: Topical Studies in Oceanography*, **56 (13)**, 778–795, https://doi.org/10.1016/j.dsr2.2008.10.033, Southern Ocean Shelf Slope Exchange.

Pan, L., E. M. Powell, K. Latychev, J. X. Mitrovica, J. R. Creveling, N. Gomez, M. J. Hoggard, and P. U. Clark, 2021: Rapid postglacial rebound amplifies global sea level rise following west Antarctic ice sheet collapse. *Science Advances*, **7 (18)**, eabf7787, https://doi.org/10.1126/sciadv.abf7787.

Paolo, F. S., H. A. Fricker, and L. Padman, 2015: Volume loss from Antarctic ice shelves is accelerating. *Science*, **348 (6232)**, 327–331, https://doi.org/10.1126/science.aaa0940.

Pritchard, H., S. Ligtenberg, H. Fricker, D. Vaughan, M. Van den Broeke, and L. Padman, 2012: Antarctic ice-sheet loss driven by basal melting of ice shelves. *Nature*, **484**, 502–5, https://doi.org/10.1038/nature10968.

Redi, M. H., 1982: Oceanic isopycnal mixing by coordinate rotation. *Journal of Physical Oceanography*, **12 (10)**, 1154 – 1158, https://doi.org/10.1175/1520-0485(1982)012⟨1154:OIMBCR⟩2.0.CO;2.

Rignot, E., and S. S. Jacobs, 2002: Rapid bottom melting widespread near Antarctic ice sheet grounding lines. *Science*, **296 (5575)**, 2020–2023, https://doi.org/10.1126/science.1070942.

Rignot, E., J. Mouginot, M. Morlighem, H. Seroussi, and B. Scheuchl, 2014: Widespread, rapid grounding line retreat of Pine Island, Thwaites, Smith, and Kohler glaciers, West Antarctica, from 1992 to 2011. *Geophysical Research Letters*, **41 (10)**, 3502–3509, https://doi.org/10.1002/2014GL060140.

Rignot, E., J. Mouginot, B. Scheuchl, M. van den Broeke, M. J. van Wessem, and M. Morlighem, 2019: Four decades of Antarctic ice sheet mass balance from 1979–2017. *Proceedings of the National Academy of Sciences*, **116 (4)**, 1095–1103, https://doi.org/10.1073/pnas.1812883116.

Ryan, S., T. Hattermann, E. Darelius, and M. Schröder, 2017: Seasonal cycle of hydrography on the eastern shelf of the Filchner Trough, Weddell Sea, Antarctica. *Journal of Geophysical Research: Oceans*, **122 (8)**, 6437–6453, https://doi.org/https://doi.org/10.1002/2017JC012916.

Schmidt, G. A., C. M. Bitz, U. Mikolajewicz, and L.-B. Tremblay, 2004: Ice-ocean boundary conditions for coupled models. *Ocean Model.*, **7**, 59–74, https://doi.org/10.1016/S1463-5003(03)00030-1.

Si, Y., A. L. Stewart, and I. Eisenman, 2022: Coupled ocean–sea ice dynamics of the Antarctic Slope Current driven by topographic eddy suppression and sea ice momentum redistribution. *Journal of Physical Oceanography*, **52 (7)**, 1563 – 1589, https://doi.org/10.1175/JPO-D-21-0142.1.

Si, Y., A. L. Stewart, and I. Eisenman, 2023: Heat transport across the Antarctic Slope Front controlled by cross-slope salinity gradients. *Science Advances*, **9 (18)**, eadd7049, https://doi.org/10.1126/sciadv.add7049.

St-Laurent, P., J. M. Klinck, and M. S. Dinniman, 2013: On the role of coastal troughs in the circulation of warm circumpolar deep water on Antarctic shelves. *Journal of Physical Oceanography*, **43 (1)**, 51 – 64, https://doi.org/10.1175/JPO-D-11-0237.1.

Stewart, A., and A. Thompson, 2015: Eddy-mediated transport of warm circumpolar deep water across the Antarctic shelf break. *Geophysical Research Letters*, **42**, https://doi.org/10.1002/2014GL062281.

Stewart, A., and A. Thompson, 2016: Eddy generation and jet formation via dense water outflows across the Antarctic continental slope. *Journal of Physical Oceanography*, **46**, https://doi.org/10.1175/JPO-D-16-0145.1.

Stewart, A. L., 2021: Mesoscale, tidal, and seasonal/interannual drivers of the Weddell Sea overturning circulation. *Journal of Physical Oceanography*, **51 (12)**, 3695 – 3722, https://doi.org/10.1175/JPO-D-20-0320.1.

Stewart, A. L., A. Klocker, and D. Menemenlis, 2018: Circum-Antarctic shoreward heat transport derived from an eddy- and tide-resolving simulation. *Geophysical Research Letters*, **45 (2)**, 834–845, https://doi.org/10.1002/2017GL075677.

Stewart, A. L., and A. F. Thompson, 2013: Connecting Antarctic cross-slope exchange with Southern Ocean overturning. *Journal of Physical Oceanography*, **43 (7)**, 1453 – 1471, https://doi.org/10.1175/JPO-D-12-0205.1.

Stone, P. H., 1972: A simplified radiative-dynamical model for the static stability of rotating atmospheres. *Journal of Atmospheric Sciences*, **29 (3)**, 405 – 418, https://doi.org/10.1175/1520-0469(1972)029⟨0405:ASRDMF⟩2.0.CO;2.

Thompson, A., K. Heywood, S. Schmidtko, and A. Stewart, 2014: Eddy transport as a key component of the Antarctic overturning circulation. *Nature Geoscience*, **7**, 879–884, https://doi.org/10.1038/ngeo2289.

Thompson, A., A. Stewart, P. Spence, and K. Heywood, 2018: The Antarctic Slope Current in a changing climate. *Reviews of Geophysics*, **56**, https://doi.org/10.1029/2018RG000624.

Thompson, A. F., and K. J. Heywood, 2008: Frontal structure and transport in the northwestern Weddell Sea. *Deep Sea Research Part I: Oceanographic Research Papers*, **55 (10)**, 1229–1251, https://doi.org/10.1016/j.dsr.2008.06.001.

Vernet, M., and Coauthors, 2019: The Weddell Gyre, Southern Ocean: Present knowledge and future challenges. *Reviews of Geophysics*, **57 (3)**, 623–708, https://doi.org/10.1029/2018RG000604.

Visbeck, M., J. Marshall, T. Haine, and M. Spall, 1997: Specification of eddy transfer coefficients in coarse-resolution ocean circulation models. *Journal of Physical Oceanography*, **27 (3)**, 381 – 402, https://doi.org/10.1175/1520-0485(1997)027⟨0381:SOETCI⟩2.0.CO;2.

Wang, Q., S. Danilov, E. Fahrbach, J. Schröter, and T. Jung, 2012: On the impact of wind forcing on the seasonal variability of Weddell Sea Bottom Water transport. *Geophysical Research Letters*, **39 (6)**, https://doi.org/10.1029/2012GL051198.

Wang, Q., S. Danilov, H. Hellmer, D. Sidorenko, J. Schröter, and T. Jung, 2013: Enhanced cross-shelf exchange by tides in the western Ross Sea. *Geophysical Research Letters*, **40**, 5735–5739, https://doi.org/10.1002/2013GL058667.

Wang, Y., and A. L. Stewart, 2020: Scalings for eddy buoyancy transfer across continental slopes under retrograde winds. *Ocean Modelling*, **147**, 101 579, https://doi.org/10.1016/j.ocemod.2020.101579.

Wei, H., and Y. Wang, 2021: Full-depth scalings for isopycnal eddy mixing across continental slopes under upwelling-favorable winds. *Journal of Advances in Modeling Earth Systems*, **13 (6)**, e2021MS002 498, https://doi.org/10.1029/2021MS002498.

Wei, H., Y. Wang, A. L. Stewart, and J. Mak, 2022: Scalings for eddy buoyancy fluxes across prograde shelf/slope fronts. *Journal of Advances in Modeling Earth Systems*, **14 (12)**, e2022MS003 229, https://doi.org/10.1029/2022MS003229, e2022MS003229 2022MS003229.

Williams, G. D., S. Aoki, S. S. Jacobs, S. R. Rintoul, T. Tamura, and N. L. Bindoff, 2010: Antarctic Bottom Water from the Adélie and George V Land coast, East Antarctica (140–149°e). *Journal of Geophysical Research: Oceans*, **115 (C4)**, https://doi.org/10.1029/2009JC005812.

Winton, M., R. Hallberg, and A. Gnanadesikan, 1998: Simulation of density-driven frictional downslope flow in z-coordinate ocean models. *Journal of Physical Oceanography*, **28 (11)**, 2163 – 2174, https://doi.org/10.1175/1520-0485(1998)028⟨2163:SODDFD⟩2.0.CO;2.

Wåhlin, A. K., R. D. Muench, L. Arneborg, G. Björk, H. K. Ha, S. H. Lee, and H. Alsén, 2012: Some implications of Ekman layer dynamics for cross-shelf exchange in the Amundsen Sea. *Journal of Physical Oceanography*, **42 (9)**, 1461 – 1474, https://doi.org/10.1175/JPO-D-11-041.1.